ingegneria sismica
International Journal of Earthquake Engineering
Anno XLIII - Num. 1 - 2026

Research on Ultrasonic Total Focusing and Phase Coherence Factor Imaging

Kaida Feng[1], *Lianlian Xin*[1], *Kunnian Pan*[1], *Xiaozhao Zhou*[1], *Bin Shao*[2], *Chunhua Fang*[2,*] *and Zekun Zheng*[2]

[1] Guangdong Power Grid Yangjiang Power Supply Company, No. 110, Mojiang Road, Yangjiang, Guangdong, 529500, China
[2] College of Electricity and New Energy, China Three Gorges University,No. 8, Daxue Road, Yichang, Hubei 443002, China

SUMMARY: *This study applies the phase coherence imaging (PCI) post-processing algorithm to the ultrasonic phased array total focusing method (TFM) to effectively improve the low signal-to-noise ratio (SNR) level of TFM imaging. Initially, a carbon steel block model was established in COMSOL software to obtain full matrix simulation data. Subsequently, by using MATLAB, circular coherence factor (CCF), sign coherence factor (SCF), sign coherence weighting (SCW), and instantaneous phase coherence factor (IPCF) were constructed to characterize the phase coherence of signals at each point in the full matrix. Following this, these factors were combined with the TFM imaging algorithm to compare their noise reduction and artifact removal effects, through which the optimal phase coherence factor was obtained. Furthermore, experimental validation was peformed, and the optimal phase coherence factor was further enhanced in dB amplitude to form the TFM-CCF-dB imaging algorithm. The results show that TFM-CCF-dB can eliminate image noise and artifacts while enhancing the amplitude of defect signals, thus improving the imaging SNR and detection accuracy.*

KEYWORDS: *Ultrasound total focusing; Phase coherence factor; Noise reduction.*

1 Introduction

1.1 A Subsection Sample

In 2005, Holmes et al. first proposed the Total Focusing Method (TFM), which is an image reconstruction method based on Full Matrix Capture (FMC) data processed using the total focusing algorithm. This method has become a research focus due to its high measurement accuracy, precise defect localization, minimal imaging blind spots, and high algorithmic flexibility, earning the title of the "golden rule" in ultrasonic imaging. Despite its renowned detection precision, the amplitude superposition process can incorrectly add reflection echo data from different defects to non-corresponding locations, introducing noise and artifacts into the imaging. Hence, combining the TFM algorithm with advanced noise reduction algorithms has become an effective strategy to further reduce noise and artifacts, thereby significantly enhancing image precision and accuracy.

Zhang et al. skillfully applied instantaneous phase coherence factors and instantaneous phase weighting factors to weight the Green's function, innovatively introducing a power

*fang107531@163.com
https://doi.org/10.65102/is20261024
Published: 30 April, 2026

exponent into the instantaneous phase coherence factor. This strategy effectively restores the original signal information and significantly reduces background noise interference, thereby greatly enhancing the SNR level. Xie et al. proposed a novel phase coherence coefficient-weighted TFM imaging technique combined with threshold fusion, which not only simplifies the model complexity but also significantly enhances the accuracy of quantitative analysis of defect size and the SNR performance of the image. Chen Yao et al. introduced the circular coherence factor (CCF) and sign coherence factor (SCF), which improved the SNR of TOFD imaging for thick-walled welds. Xu Songbai integrated the instantaneous phase coherence factor (IPCF) and sign coherence weighting (SCW) into the TFM imaging algorithm, thereby eliminating image artifacts and enhancing image SNR.

The phase coherence factors used in the aforementioned studies effectively remove image noise and artifacts, improving the accuracy of detection images. To identify the phase coherence factor with the best denoising effect, this paper compares the noise reduction performances of these factors and applies the CCF, SCF, IPCF, and SCW factors sequentially to the signal data in the full matrix. Specifically, COMSOL finite element simulation software was first used to analyze the propagation characteristics and patterns of ultrasound in carbon steel blocks, achieving sequential “single-element transmission with full-array reception” for all elements using the parametric sweeping function to obtain the full matrix data of the carbon steel block. Then, the four factors were combined with the TFM imaging algorithm to compare the effects of noise and artifact reduction, resulting in the identification of the optimal phase coherence factor. Experimental verification was then conducted, and the optimal phase coherence factor was further enhanced by dB amplitude to form the TFM-CCF-dB imaging algorithm, which improves image SNR and accuracy.

2 Principles of Total Focusing and Phase Coherence Algorithms

2.1 Principles of Total Focusing Imaging Algorithm

The Total Focusing Method is a post-processing imaging algorithm based on full matrix data. For an ultrasonic phased array probe with N elements, following the excitation rule of sequential "single-element transmission with full-array reception" for each element, a full matrix of $N \times N$ A-scan signals is collected. This full matrix data serves as the foundational data source for the ultrasonic total focusing imaging algorithm, comprehensively covering all acoustic wave information in the inspected area. TFM first divides the detection area into a grid of focal points, then calculates the delay times from the transmitting element *i* to the focal point *P*, and then to the receiving element *j*, based on sound speed and path, performing amplitude index superposition. The acoustic wave amplitude *I(x,z)* at the focal point is then obtained. The processing is completed sequentially for all focal points according to the above steps, and imaging is performed based on the amplitude matrix. The principle of total focusing is shown in Equation (1).

$$I_p(x_p, z_p) = \sum_{i=1}^{N} \sum_{j=1}^{N} A_{ij}\left(t_{ij}(x_p, z_p)\right) \tag{1}$$

$$t_{ij}(x_p, z_p) = \frac{\left(\sqrt{(x_i - x_p)^2 + z_p^2} + \sqrt{(x_j - x_p)^2 + z_p^2}\right)}{c} \tag{2}$$

where, $t_{ij}(x_p, z_p)$ represents the time required for the ultrasound emitted from element i to propagate to point P, and then for the echo reflected from P to be received by element j. c is the speed of sound in the object being inspected.

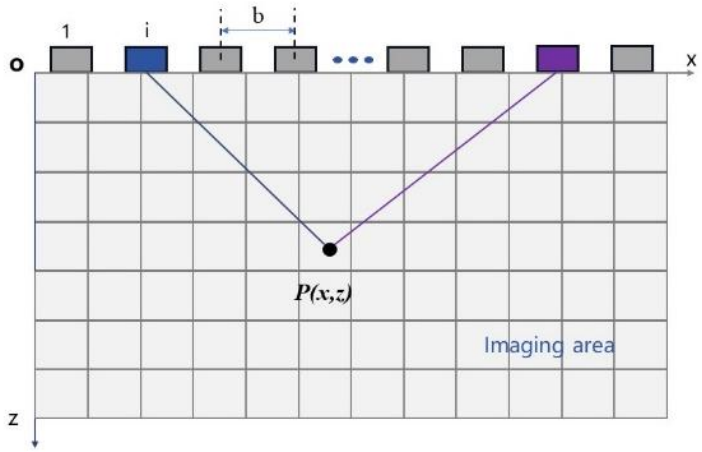

Figure 1: Schematic of total focused imaging algorithm

	1	…	j	…	n
1	S_{11}	…	S_{1j}	…	S_{1n}
⋮	⋮	⋮	⋮	⋮	⋮
j	S_{i1}	…	S_{ij}	…	…
⋮	⋮	⋮	⋮	⋮	⋮
n	S_{n1}	…	…	…	S_{nn}

Figure 2: Schematic of the captured full matrix data

2.2 Principles of Phase Coherence Imaging

Phase coherence imaging is an algorithm that uses the phase distribution of received echo signals to construct weighting factors for the weighted reconstruction of images. The echo phase distribution at defect locations in the full matrix data is consistent and well-aligned, indicating high phase coherence. In contrast, the phase distribution of noise in the echoes is random and discrete, indicating low phase coherence. Based on this principle, phase information from the full matrix signals can be extracted to construct the corresponding phase coherence factors, and the image matrix formed by the TFM method can be weighted using this phase coherence factor $C(x,z)$.

$$I_C(x,z) = \left| C(x,z) I(x,z) \right| \tag{3}$$

Phase coherence factors are functions constructed based on the phase standard deviation of each pixel in the image. Therefore, the phase distribution of noise in the image is random and has a high standard deviation, resulting in a low phase coherence factor. As a result, the amplitude of the I_C after weighted reconstruction is reduced, thereby decreasing the amplitude

of the noise. Conversely, when the standard deviation is low, the corresponding phase coherence factor value is high, and the amplitude of the pixel after weighted reconstruction remains relatively constant. Consequently, noise signals in the weighted reconstructed image matrix can be effectively removed.

3 Simulation Model and Imaging of Simulation Data

3.1 Construction of Simulation Model

To investigate the effects of different phase coherence factors on defect detection imaging in a carbon steel block, a two-dimensional cross-sectional model of a 50 mm×70 mm carbon steel block was created using COMSOL finite element software. The speed of sound in carbon steel is 5900 m/s, with a density of 7.9g/cm³. Coupling agents were used to ensure effective coupling between the model and the array elements, with 0.5 mm diameter circular hole defects placed at various positions within the carbon steel block to investigate the imaging effects of defects at different locations.

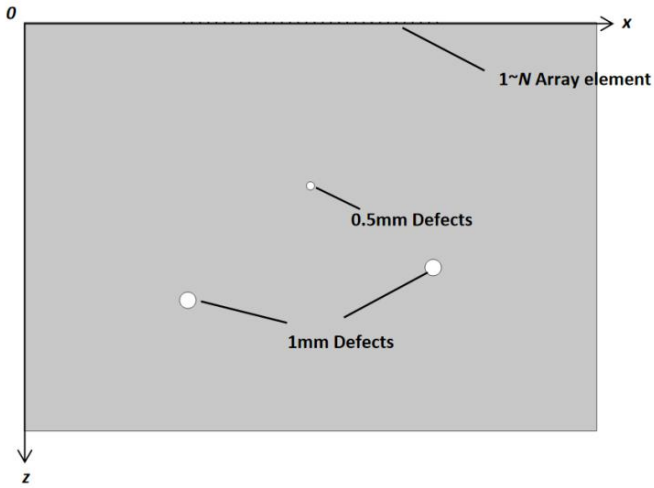

Figure 3: Schematic of the total-focus imaging algorithm

The model employs a pressure acoustics physics field to calculate the propagation of the sound field within the carbon steel block. Instantaneous pressure is applied in the y-axis direction to the top line segment of the model to simulate the excitation of actual ultrasonic probe signals, with the boundary of the lower semicircle set as a plane wave radiation boundary condition to ensure that the ultrasound is absorbed and not reflected at this boundary. The maximum element size of the mesh is defined as 1/5 of the material wavelength, with a time step of 0.01 μs and a total simulation duration of 30 μs. To obtain the full matrix data, parametric sweeping in COMSOL is used to achieve sequential "single transmission with full-array reception" for all elements. After the calculations are completed, the full matrix data of N×N sets can be obtained, which can then be used to analyze the effects of different phase factors on the imaging of subtle defects in the carbon steel block.

With a probe frequency of 5MHz and 64 elements, and an element spacing of 1mm, the total focusing imaging of this simulation model is shown in Figure 4. The top of the image shows a surface blind spot caused by the non-uniform sound pressure distribution in the near-field region of the ultrasonic probe. The three circular holes in the center are the imaging of three defects in the model. The red area at the bottom represents the model's bottom surface.

Also, there is background noise present near the defects and the bottom surface. To further improve image accuracy, phase coherence factors are introduced to reduce noise.

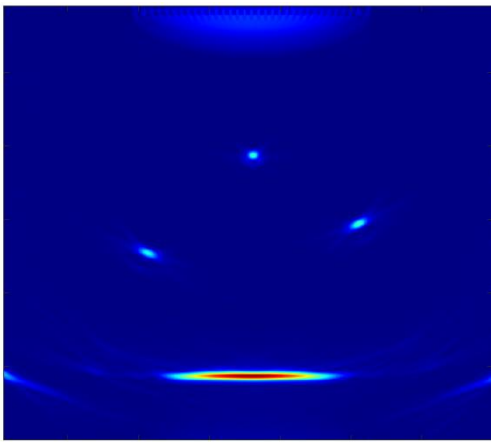

Figure 4: Schematic of TFM simulation imaging

3.2 Total Focusing Simulation Imaging with Different Phase Coherence Factors

Circular Coherence Factor. The calculation process for the Circular Coherence Factor (CCF) is as follows:

First, apply the Hilbert transform to the full matrix signals to extract phase information, using the formula:

$$h(t) = |h| e^{i\varphi} = |h| (\cos\varphi + j \sin\varphi) \tag{4}$$

where, $|h|$ is the modulus of the signal, φ is the phase angle of the signal, and the phase information of the real and imaginary parts of the signal is represented by sine and cosine, respectively.

Then, based on Equations (5) and (6), the phase information and phase standard deviation *var(cosφ)* and *var(sinφ*) corresponding to each pixel are calculated.

$$\mathrm{var}(\sin\varphi(x,z,i)) = \frac{1}{N}\sum_{i=1}^{N} \sin^2\varphi - (\frac{1}{N}\sum_{i=1}^{N} \sin\varphi)^2 \tag{5}$$

$$\mathrm{var}(\cos\varphi(x,z,i)) = \frac{1}{N}\sum_{i=1}^{N} \cos^2\varphi - \left(\frac{1}{N}\sum_{i=1}^{N} \cos\varphi\right)^2 \tag{6}$$

$$\mathrm{C}_{CCF}(x,z) = 1 - \mathrm{sqr}t[\mathrm{var}(\cos\varphi) + \mathrm{var}(\sin\varphi)] \tag{7}$$

where, *var(cosφ) and var(sinφ)* are functions of pixel coordinates *(x,z)* and step position *i*. *sqrt[var(cosφ)+var(sinφ)]* represents the phase standard deviation of each pixel in the image matrix.

Next, based on Equation (7), calculate and normalize the Circular Coherence Factor (CCF) for each pixel. After normalization, the value range of C_{CCF} is [0,1]; the smaller the factor, the worse the coherence; and the larger the factor, the better the coherence. Finally, use the C_{CCF} factor to perform weighted reconstruction on the image matrix *I(x,z)*, obtaining a new image matrix $I_C(x,z)$.

The simulated imaging after weighting with the C_{CCF} factor is shown in Figure 5, where noise in the surface blind spot, near defects, and near the bottom surface of the entire image has been eliminated, achieving good noise reduction. The defect shapes are smooth and undistorted.

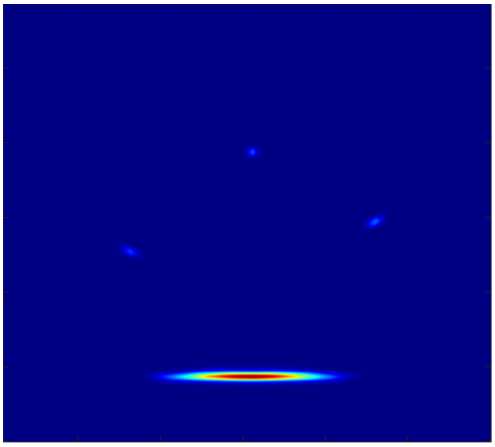

Figure 5: Schematic of TFM-CCF simulated imaging

Sign Coherence Weighting. Based on the phase polarization standard deviation of array signals, the Sign Coherence Factor (SCF) can be constructed, and its expression is as follows:

$$C_{SCF}(x,z) = 1 - \sqrt{\mathrm{var}[sign(\cos\varphi)]} \tag{8}$$

In the formula, sign(·) is the sign function, where its value is 1 if the phase $cos\varphi$ is positive, -1 if negative, and 0 if zero.

The simulated imaging after weighting with the C_{SCF} factor is shown in Figure 6. It can be observed that the surface blind spot and noise in the entire image have been eliminated, indicating a good noise reduction effect. However, distortion of the defects has occurred.

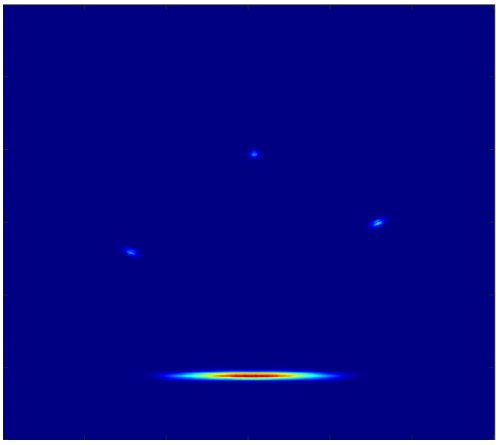

Figure 6: Schematic of TFM-SCF simulated imaging

Sign Coherence Weighting. This weighting method first involves using a Butterworth digital band-pass filter to filter the full data matrix S, obtaining matrix S', which eliminates DC components and reduces the impact of background noise on imaging results, as expressed in the following equation:

$$W_{SCW}(x,z)=\frac{1}{N^2}\left\{\sum_{i=1}^{N}\sum_{j=1}^{N}b_{ij}(x,z)\right\}^{\tau} \tag{9}$$

where $b_{ij}(x,z)$ represents the sign (positive or negative, polarity) of the data corresponding to point $P(x,z)$ in the signal received by element j from the signal excited by element i. $S(t)$ is the captured full matrix signal, and according to the unit step function, when $S'(t)>0$, $b_{ij}=1$; when $S'(t)<0$, $b_{ij}=-1$; when $S'(t)=0$, $b_{ij}=0$. $t_{ij}(x_p,z_p)$ is the time required for ultrasound to propagate from element i to point P, and for the echo reflected from P to be received by element j. The parameter is used to adjust the sensitivity of the weighting factor; generally, the larger the value, the more significant the effect of sign coherence weighting, and the more prominent the noise suppression. However, an excessively large value is not appropriate. It has been verified that the optimal range for this value is between 1 and 2, with 1.5 being the generally optimal choice.

The simulated imaging after weighting with the W_{SCW} factor is shown in Figure 7. Clearly, the surface blind spot of the entire image has been eliminated; however, some noise remains near the defects and the bottom surface, and the imaging of defects and the bottom surface exhibits more pronounced distortion.

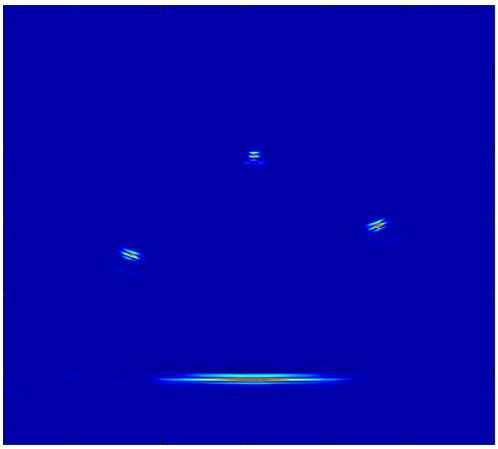

Figure 7: Schematic of TFM-SCW simulated imaging

Instantaneous Phase Coherence. The Instantaneous Phase Coherence Factor (W_{IPCF}) treats A-scan signals as sinusoidal phase-modulated signals where the amplitude is related to time t. By analyzing the phase characteristics of A-scan signals at specific grid points, corresponding compensation coefficients are determined. W_{IPCF} can eliminate image artifacts and improve the image's SNR, demonstrating strong denoising capabilities. To extract the required phase information, the matrix must first undergo Hilbert transform processing, followed by the application of Euler's formula to extract the phase information from the A-scan signals, with the specific formula given by:

$$H[S_{ij}(\mathrm{t})]=|h|e^{j\varphi_{ij}}=|h|(\cos\varphi_{ij}+j\sin\varphi_{ij}) \tag{10}$$

$$W_{IPCF}(x,z)=\frac{1}{N^2}\left\{\begin{array}{l}\left[\sum_{i=1}^{N}\sum_{j=1}^{N}\cos\varphi i_j(x,z)\right]^2\\ +\left[\sum_{i=1}^{N}\sum_{j=1}^{N}\sin\varphi_{ij}(x,z)\right]^2\end{array}\right\} \tag{11}$$

The simulated imaging after weighting with the W_{IPCF} factor is shown in Figure 8. It can be seen that the surface blind spot and noise in the entire image have been eliminated, resulting in effective noise reduction. However, the amplitude of the defects is also weakened during the denoising process, leading to a fainter and slightly distorted defect image.

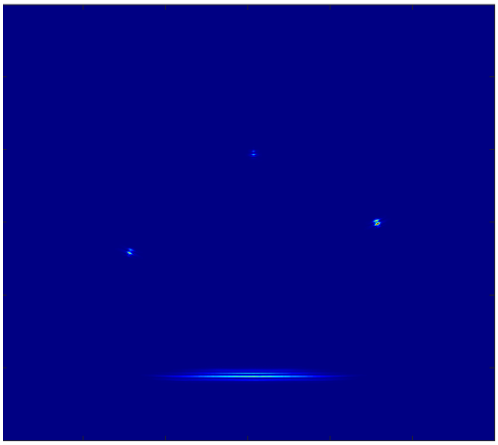

Figure 8: Schematic of TFM-IPCF simulated imaging

4 Experimental Verification

4.1 Construction of the Test Sample and Experimental Platform

To validate the correctness of the simulation and algorithm, a Type B ultrasonic phased array test block was selected as the test object. This block, made of carbon steel, is an international standard block used for calibrating and measuring the defect resolution of phased array ultrasonic flaw detectors. The block contains 18 circular hole defects arranged in an arc at various positions. The ultrasonic phased array system used is the 64-channel fully parallel phased array total focusing method (TFM) real-time ultrasonic imaging detection system CTS-PA32BM from Guangdong Shantou Ultrasound Company. The number of sampling points is 16,384. The phased array probe parameters are 5 MHz, 64 elements, with a 1mm element pitch (also from Guangdong Shantou Ultrasound Company). The ultrasonic total focusing detection platform is shown in Figure 9.

(a) photo of the detection platform (b)Detail view

Figure 9: Ultrasonic total-focus inspection platform

As shown in Figure 10, the TFM imaging results exhibit a noticeable blind zone at the top due to difficulties in achieving perfect contact between the carbon steel block and the probe,

uneven pressure distribution in the ultrasonic near-field region, and limitations in the equipment's performance. Although the total focusing algorithm successfully captured and displayed all 18 defects, defects 1, 2, and 3 near the surface appear blurred due to the blind zone. Additionally, significant noise around the defects and in the lower-left corner of the image results in an overall lack of smoothness.

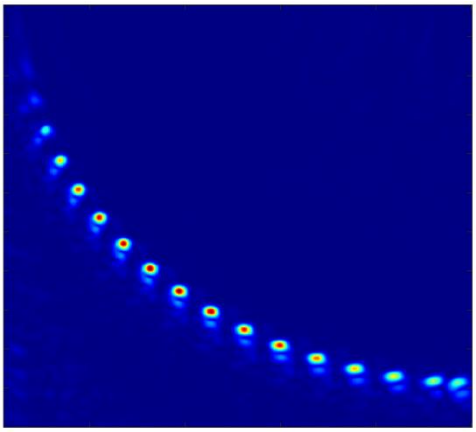

Figure 10: Schematic of TFM Experimental Imaging

4.2 Total Focusing Experimental Imaging with Different Phase Coherence Factors

Circular Coherence Factor. The imaging of TFM-CCF is shown in Figure 11, where the TFM-CCF algorithm demonstrates superior denoising performance compared to TFM, effectively smoothing the image and removing artifacts without any distortion of defect images. The defect imaging is comprehensive and aesthetically pleasing, closely matching the actual defect shapes. However, the signals for defects 1, 2, and 3 near the surface, as well as defects 17 and 18 in the distant region, are relatively weak. Overall, the imaging performance is good.

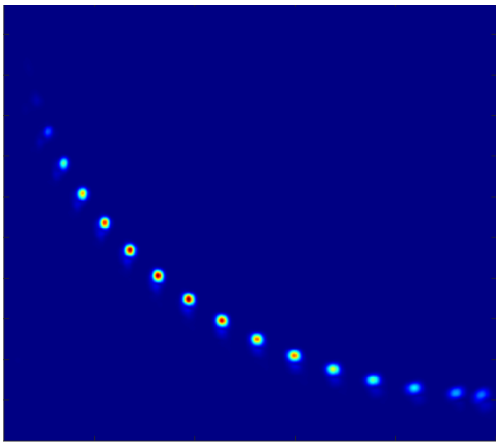

Figure 11: Schematic of TFM-CCF Experimental Imaging

Sign Coherence Weighting. The imaging of TFM-SCF is shown in Figure 12. Compared to TFM, the TFM-SCF algorithm, offers superior denoising performance, effectively smoothing images and removing artifacts, while providing a better representation of defect shapes. Its noise and artifact reduction performance is similar to that of TFM-CCF. However, compared to TFM-CCF, the signal amplitudes of defects 1, 2, 3, 16, 17, and 18 are further reduced, resulting in weaker defect imaging. Additionally, slight distortion appears in the defect imaging,

and the overall imaging performance is not as good as that of TFM-CCF.

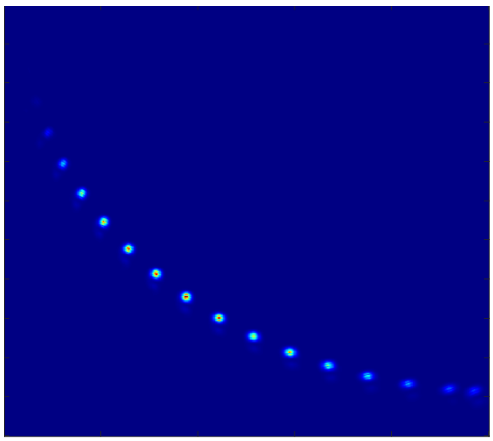

Figure 12: Schematic of TFM-SCF Experimental Imaging

Sign Coherence Weighting. The imaging of TFM-SCW is shown in Figure 13. The TFM-SCW algorithm, compared to TFM, exhibits excellent denoising performance, effectively improving image SNR and removing artifacts, while providing a better representation of defect shapes. Its noise and artifact reduction performance is similar to TFM-CCF. However, compared to TFM-CCF, some defect signal amplitudes are further reduced, and the imaging of defects experiences severe distortion, resulting in an uneven image with weaker defect representation. Overall, the imaging performance is not as good as that of TFM-CCF.

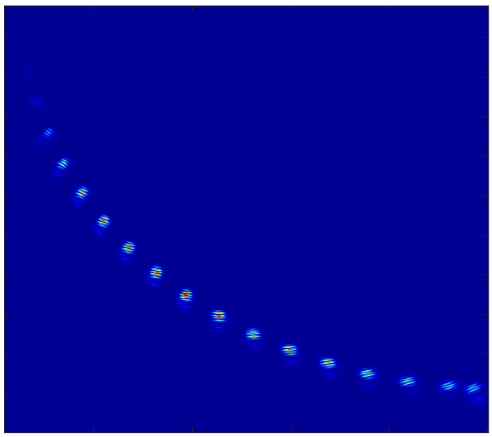

Figure 13: Schematic of TFM-SCW Experimental Imaging

Instantaneous Phase Coherence. The imaging of TFM-IPCF is shown in Figure 14. Compared to the TFM algorithm, the TFM-IPCF algorithm demonstrates strong denoising capabilities, efficiently eliminating noise and removing artifacts in the image. However, the overall defect imaging performance of TFM-IPCF is poor. While it removes noise and artifacts, it also significantly weakens all defect imaging, making them very faint and distorted, resulting in an overall inferior imaging effect compared to TFM-CCF.

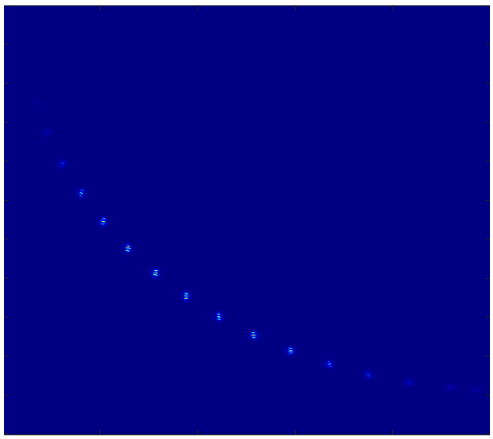

Figure 14: Schematic of TFM-IPCF Experimental Imaging

Circular Coherence Factor with dB Amplitude Enhancement. The execution process of the dB amplitude enhancement algorithm is as follows: First, an average dB threshold (k) for the image matrix is set. Then, the dB value of each point in the image matrix is calculated, and these values are compared with the preset average threshold (k). For all dB values less than k, they are set to 0, while those greater than k remain unchanged.

As observed in Figure 15, in TFM-CCF-dB imaging, although defect 1 near the surface is not visible, noise artifacts around defects at all positions have been significantly reduced. Additionally, by integrating the three algorithms of TFM-CCF-dB, defects 3, 17, and 18 in the imaging are significantly enhanced, effectively addressing the issue of insufficient defect clarity in TFM-CCF imaging. Compared to the TFM-CCF algorithm, TFM-CCF-dB not only retains the advantages of TFM-CCF in reducing noise and artifacts but also further enhances defect visibility, making them more prominent. Therefore, TFM-CCF-dB exhibits superior noise suppression performance, significantly improving image smoothness and accuracy, and is more effective in eliminating artifacts around image defects.

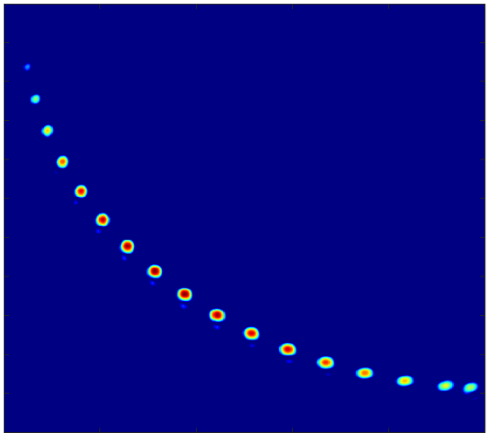

Figure 15: Schematic of TFM-CCF-dB Experimental Imaging

References

[1] Holmes C, Drinkwater B W, Wilcox P D. Post-processing of the full matrix of ultrasonic transmit-receive array data for nondestructive evaluation. NDT and E International, 2005, 38(8): 701-711.

[2] Hunter A J, Drinkwater B W, Wilcox P D. The wavenumber algorithm for full-matrix imaging using an ultrasonic array. IEEE transactions on ultrasonics, ferroelectrics, and frequency control, 2008, 55(11): 2450-2462.

[3] Liu Zhao, Kang Zhiyuan, Zhang Xianglin, et al. Application of total focusing imaging technology in thin plate weld inspection. Nondestructive Testing, 2018, 42(4): 3. (in Chinese)

[4] Yang Shian. Design of real-time total focusing system for ultrasonic phased array based on FPGA. University of Chinese Academy of Sciences, 2023-12-21. (in Chinese)

[5] Yang Guide, Chen Wei, Zhan Hongqing, et al. Denoising of phased array total focusing images based on wavelet transform. Nondestructive Testing, 2018, 40(08): 53-56. (in Chinese)

[6] Zhang H, Zeng L, Fan G, et al. Instantaneous phase coherence imaging for near-field defects by ultrasonic phased array inspection. Sensors, 2020, 20(3): 775.

[7] Xie Y, Zhou L, Zhang X, et al. Weighted full-focus defect detection and imaging method based on threshold fusion for phase coherence factor. Journal of Sensors, 2022, 2022: 1-14.

[8] Chen Yao, Mao Qiuqin, Shi Wenze, et al. Research on TOFD imaging detection of thick-walled welds based on phase coherence. Journal of Mechanical Engineering, 2019, 55(04): 25-32. (in Chinese)

[9] Xu Songbai. Research on total focusing algorithm based on phase weighting and correction compensation. Southwest Jiaotong University, 2022. DOI:10.27414/d.cnki. gxnju.2022.001249. (in Chinese)

[10] Xu Na, Xu Lulu, He Fangcheng. Ultrasonic array total focusing imaging of anisotropic additive manufacturing components. Journal of Beihang University, 2023, 49(05): 1063-1070. (in Chinese)

[11] Chen Feng, et al. Quantitative method for rail defects based on ultrasonic phased array total focusing DAC spectrum. Journal of Mechanical Engineering, 2021, 57(18): 32-41. (in Chinese)

[12] Camacho J, Fritsch C, Fernandez-Cruza J, et al. Phase Coherence Imaging: Principles, applications, and current developments. 178th Meeting of the Acoustical Society of America, 2019.

[13] Mao Qiuqin, Chen Yao, Shi Wenze, et al. Research on frequency domain phase coherence synthetic aperture focused ultrasonic imaging. Journal of Instrumentation, 2020, 41(02): 135-145. (in Chinese)

[14] Kang Da, Chen Yao, Jin Shijie, et al. Research on TOFD defect image enhancement processing based on phase coherence imaging. Pressure Vessels, 2016, 33(06): 59-66. (in Chinese)

[15] Chen Yao. Modeling and PCI denoising algorithm research for thick-walled CASS

ultrasonic testing. Dalian University of Technology, 2017. (in Chinese)

[16] Mao Qiuqin, Chen Yao, Shi Wenze, et al. Research on frequency domain phase coherence synthetic aperture focused ultrasonic imaging. Journal of Instrumentation, 2020, 41(02): 135-145. DOI:10.19650/j.cnki.cjsi.J1905868. (in Chinese)

[17] Long Shengrong, Chen Yao, Kong Qingru, et al. Frequency domain coherent composite plane wave imaging weighted by sign coherence factor in double-layer media. Journal of Instrumentation, 2022, 43(03): 32-39. DOI:10.19650/j.cnki.cjsi.J2108264. (in Chinese)

[18] Zhang Haoqian, Zhao Kai. Research on ultrasonic phased array defect imaging and classification based on PCI-SVM. Progress in Laser and Optoelectronics, 2024-12-01. (in Chinese)

[19] Wang Xiang, Wang Qiang. Experimental analysis of optimized phase coherence weighted total focusing imaging for austenitic stainless steel welds. Applied Acoustics, 2024-12-01. (in Chinese)

[20] Shao Bin, Fang Chunhua, Zhou Gu, et al. Total focusing imaging based on phase coherence and dB amplitude enhancement. Acoustics Technology, 2024-11-30. (in Chinese)